

REVIEW OF RF-SAMPLE TEST EQUIPMENT AND RESULTS *

Tobias Junginger, CERN, Geneva, Switzerland and MPIK Heidelberg, Germany †

Wolfgang Weingarten, CERN, Geneva, Switzerland

Carsten Welsch, Cockcroft Institute, Warrington and University of Liverpool, United Kingdom

Abstract

A calorimetric technique enables precise measurements of the surface resistance R_S of superconducting samples. One of the devices exploiting this technique at multiple frequencies is the Quadrupole Resonator. Its measurement capabilities and limitations are discussed and compared with similar devices. Results on bulk niobium and niobium film on copper samples are presented. It is shown how different contributions to the surface resistance depend on temperature, applied RF magnetic field and frequency. Furthermore measurements of the maximum RF magnetic field as a function of temperature and frequency in pulsed and CW operation are presented.

INTRODUCTION

The surface resistance R_S of superconducting cavities can be obtained by measuring the unloaded quality factor Q_0 ,

$$R_S = \frac{G}{Q_0}, \quad (1)$$

where G is the geometry factor of the cavity, dependent only on the cavity shape and not on its size or material. G can therefore be accurately obtained by a numerical simulation. R_S may vary strongly over the cavity surface and the value obtained is an average over the whole surface [1].

A more convenient way consists of investigating small samples. They can be manufactured and duplicated at low cost. RF cavities excited in the TE_{011} mode with a sample attached as the cover plate are often used for material characterization. The TE_{011} mode is chosen, due to its convenient field configuration, i.e. no magnetic field and therefore no RF currents across the joint, where the demountable end plate sample is attached to the cavity and a vanishing electrical field over the whole cavity surface, helping to avoid multipacting, see Figure 1.

There are two techniques to derive the surface resistance of the attached sample. The first one is the end-plate replacement technique. It requires a reference sample of known surface resistance R_S . After the quality factor of the cavity with the reference sample attached has been measured the reference sample can be exchanged by another sample of unknown surface resistance. From the change in Q -value the surface resistance of the sample can be derived. For systems relying on the end-plate replacement

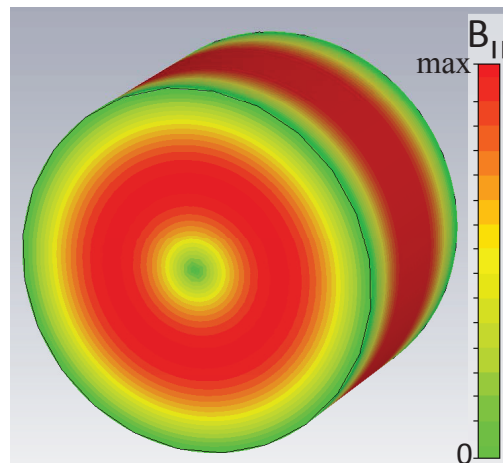


Figure 1: False color plot of the surface magnetic field $B_{||}$ in a cylindrical pillbox cavity excited in the TE_{011} mode.

technique sample, cavity and bath temperature are always identical. Therefore for these systems cavity design aims for a high magnetic field level on the sample compared to the cavity. An overview of different cavity geometries can be found in [2].

In a calorimetric system the sample and host cavity temperature are controlled independently. A DC heater (resistor) and at least one temperature sensor are attached to the backside of the sample, allowing to control its temperature.

Currently there are three calorimetric systems for the RF characterization of superconducting samples in use.

- A cylindrical TE_{011}/TE_{012} cavity enabling measurements at 4 and 5.6 GHz has been developed in collaboration between CEA Saclay and IPN Orsay [3, 4]. Recently a modified version has been constructed and commissioned [5].
- At Jefferson Laboratory (JLAB) a sapphire loaded TE_{011} cavity for measurements at 7.5 GHz has been recently commissioned [6].
- The Quadrupole Resonator at CERN is the only system running at frequencies of interest concerning accelerator applications. It has been used since more than ten years [7, 8, 9] and has been recently refurbished for measurements at 400, 800 and 1200 MHz [2].

The calorimetric technique applied by these three systems is explained in the following section. Afterwards a

* Work supported by the German Doctoral Students program of the Federal Ministry of Education and Research (BMBF)

† tobias.junginger@cern.ch

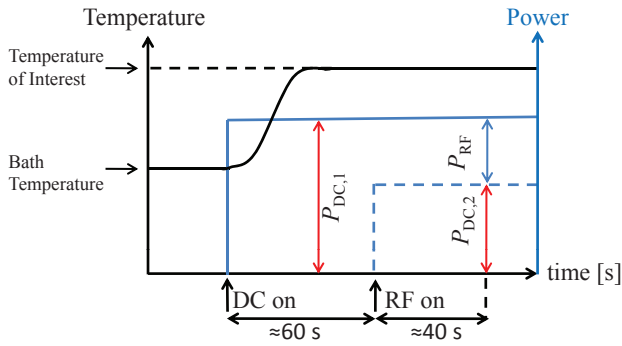


Figure 2: In a calorimetric system the surface resistance of a superconducting sample is derived from a DC measurement.

short description of each device and the results obtained by them are given.

THE CALORIMETRIC TECHNIQUE

Compared to the end-plate replacement technique, the calorimetric technique has the advantage of high sensitivity and independence of a reference sample. The drawbacks are a usually more complicated design and the fact that the measurement temperature always needs to be higher than the bath temperature.

A calorimetric measurement consists of two steps, see Figure 2:

1. The temperature is set to the temperature of interest by applying a current to the resistor on the backside of the sample. The power dissipated $P_{DC,1}$ is derived from measuring the voltage across the resistor.
2. The RF is switched on and the current applied to the resistor is lowered to keep the sample temperature and the total power dissipated constant.

The power dissipated by RF, P_{RF} is the difference between the DC power applied without RF, P_{DC1} and the DC power applied with RF, P_{DC2} . P_{RF} is directly related to the surface resistance R_S of the sample and the magnetic field on the sample surface B ,

$$P_{RF} = P_{DC1} - P_{DC2} = \frac{1}{2\mu_0^2} \int_{\text{Sample}} R_S B^2 dS. \quad (2)$$

Assuming R_S to be constant over the sample surface area and independent of B , equation (2) simplifies to

$$P_{RF} = P_{DC1} - P_{DC2} \approx \frac{1}{2\mu_0^2} R_S \int_{\text{Sample}} B^2 dS, \quad (3)$$

which can be rearranged to yield an expression for the surface resistance:

$$R_S = \frac{2\mu_0^2 (P_{DC1} - P_{DC2})}{\int_{\text{Sample}} B^2 dS}. \quad (4)$$

A constant c_1 relating the peak magnetic field on the sample surface B_p to its integrated value over the sample surface can be introduced and calculated numerically for a given mode

$$c_1 = \frac{B_p^2}{\int_{\text{Sample}} B^2 dS}. \quad (5)$$

To derive B_p from an RF measurement a second constant c_2 , relating B_p^2 to the stored energy in the cavity U is introduced. Its value must also be calculated numerically,

$$c_2 = \frac{B_p^2}{U}. \quad (6)$$

The loaded quality factor Q_L of a cavity equals

$$Q_L = \frac{\omega U}{P_L} = \omega \tau, \quad (7)$$

where the loaded power P_L is the power dissipated in the cavity and radiated into the couplers, while τ is the corresponding decay time. Inserting (6) in (7) yields

$$B_p = \sqrt{c_2 \tau P_L}. \quad (8)$$

For the Quadrupole Resonator the constants c_1 and c_2 were derived by two different computer codes, (see Table 1), based on the finite integral (CST Microwave Studio[®]) and the finite element method (Ansoft HFSS[®]). The values agree within 6%.

With the constants c_1 and c_2 (4) becomes an expression of constants and measurands:

$$R_S = 2\mu_0^2 c_1 \frac{(P_{DC1} - P_{DC2})}{c_2 \tau P_L}. \quad (9)$$

In case non critical coupling is chosen P_L must be derived from the forward and the reflected power (P_f and P_r):

$$P_L = 2P_f \mp \sqrt{P_r \times P_f}, \quad (10)$$

with minus/plus for an under/over coupled input antenna. This principle is applied in the sapphire loaded cavity equipped with two adjustable couplers [6].

The Quadrupole Resonator uses a fixed coupling instead. The device is equipped with two strongly overcoupled antennas (coupling factor ≈ 100 each). The resonator acts like a narrow band filter. Only a small, negligible amount of the power coupled in is dissipated in the resonator walls. Since the coupling geometries of the input and the output

Table 1: Field parameters of the Quadrupole Resonator calculated with CST Microwave Studio/Ansoft HFSS

f [MHz]	c_1 [1/m ²]	c_2 [T ² /J]
399.6/399.4	14.08/14.31	0.105/0.104
803.1/803.2	14.03/14.88	0.105/0.105
1211.1/1208.8	15.69/15.40	0.121/0.116

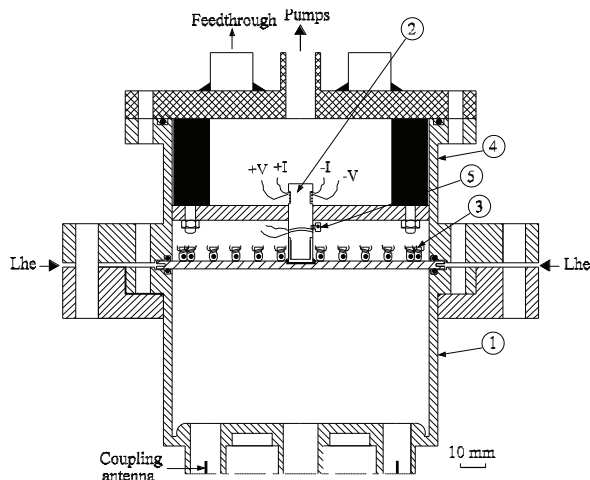


Figure 3: Experimental set-up of the TE_{011}/TE_{012} cavity (1=cylindrical cavity, 2=static heater, 3=thermometers, 4=vacuum insulation jacket, 5=calibrated thermal sensor [4]).

antenna to the resonator are identical, the coupling factor as seen from the input coupler is $\beta = 1$ (critical coupling, no power is reflected). The assumption that the input power equals the output power can be made yielding $P_f = P_t$, where P_f and P_t are the forward and the transmitted power. This allows to make the approximation $P_L = 2P_f = 2P_t$. To derive P_L it is therefore possible to measure only the transmitted power at a third sufficiently weakly coupled antenna.

The disadvantage of this setup is that Q_0 the quality factor of the cavity itself can not be measured directly. A direct comparison of the calorimetric results with a non calorimetric RF measurement can only be made if the sample is quenched and the coupling changes from strongly overcoupled to strongly undercoupled [10].

TE₀₁₁/TE₀₁₂ CAVITY FROM IPN ORSAY/CEA SACLAY

The TE_{011}/TE_{012} cavity from IPN Orsay/CEA Saclay is a cylindrical niobium cavity designed for measurements of the surface resistance of superconducting Nb and NbTiN thin films sputtered on removable copper disks.

The goal was to develop a system with improved accuracy, especially at 4 K, compared to a cylindrical niobium cavity, which used the end-plate replacement technique, relying on a reference sample. It gave a resolution of about $\pm 1000 \text{ n}\Omega$ at 4 K.

The developed calorimetric system consists of a cylindrical cavity and a thermometric part. The thermometric part is located in a vacuum insulation jacket, where a dismountable assembly with a static heater and 24 thermometers is installed, see Figure 3 [4].

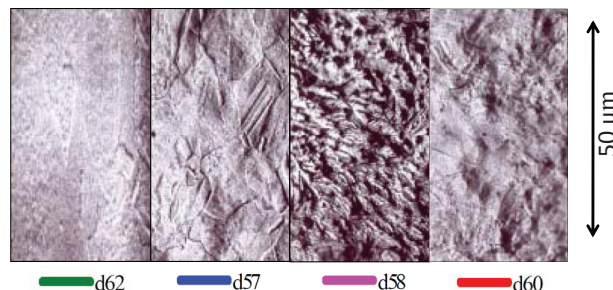
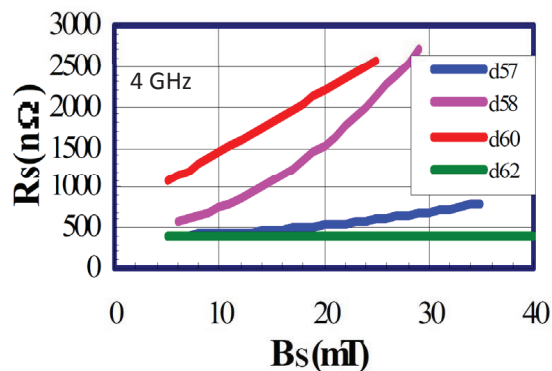


Figure 4: Top: Surface resistance of niobium on copper samples as a function of the applied magnetic field B measured at 4 GHz. Bottom: Micrographs of the sample substrates. A correlation between substrate roughness, residual resistance and resistance increase with applied field can be made [3].

The cavity has been used for systematic studies of the surface resistance of sputtered niobium on copper samples. Substrates of different roughness have been investigated. A correlation between surface roughness and surface resistance could be made, see Figure 4. The residual resistance of the thin film samples was found to scale linear with frequency [3].

Recently a modified cavity based on the same geometry has been developed for further thin film studies [5].

SAPPHIRE LOADED CAVITY FROM JEFFERSON LABORATORY

The sapphire loaded cavity was designed to measure the SRF properties of samples sufficiently small to be accommodated in commercial surface characterization instruments, surface treatment facilities and laboratory-based thin film deposition equipment.

Placing a sapphire rod in the middle of a cylindrical cavity lowers the resonant frequency, allowing to install samples of 50 mm diameter as end plate in a 7.5 GHz cavity, see Figure 5.

Being designed for thin film studies of new materials, such as Mg_2B or Nb_3Sn the cavity has been commissioned with a bulk niobium sample brazed on to a copper substrate [6].

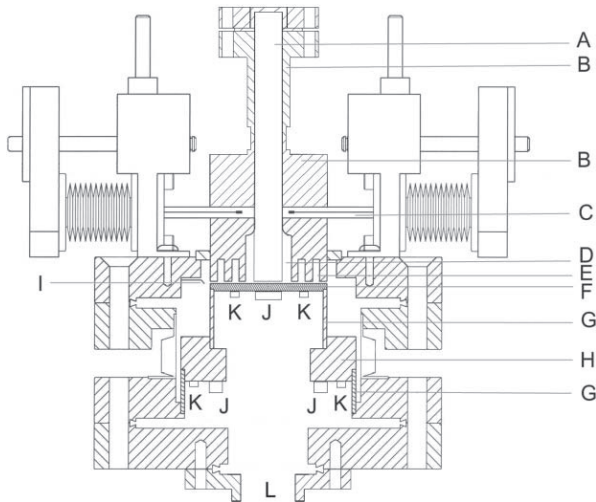


Figure 5: SIC system overview. A. Sapphire rod, B. Niobium cavity body, C. RF coupler, D. TE_{011} cavity, E. Choke joint, F. Sample on copper support plate, G. Stainless steel thermal insulator, H. Copper ring, I. RF leakage pickup coupler, J. Heater, K. Thermal sensor, L. Port for vacuum and wires. (Vacuum port of the cavity is not shown) [6].

Figures 6 and 7 depict the surface resistance R_S and the change in RF penetration depth $\Delta\lambda$ as a function of sample temperature T .

Material parameters of the sample were derived by a least squares multi-parameter fit to BCS theory [11, 12]. For a fixed critical temperature $T_c \approx 9.26$ K, the fitting parameters $\Delta/kT_c = 1.842$, London penetration depth $\lambda_L = 36.1$ nm, BCS coherence length $\xi_0 = 32.7$ nm, mean free path $\ell = 256$ nm, penetration depth at 0 K $\lambda_0 = 45.3$ nm and a residual resistance $R_{res} = 1.54 \mu\Omega$ were derived [6].

These parameters are consistent with theory and other measurements [13] and demonstrate the capability of the sapphire loaded cavity. Note that the parameters were obtained by one least squares fit to the complete data set containing the surface resistance R_S and the change in penetration depth $\Delta\lambda$.

QUADRUPOLE RESONATOR FROM CERN

The Quadrupole Resonator is a four-wire transmission line half-wave resonator using a TE_{21} -like mode.

The resonator was originally designed to measure the surface resistance of niobium film samples at 400 MHz, which are the technology and RF frequency chosen for the LHC at CERN. The device was used to measure the surface resistance at 400 MHz of bulk niobium and niobium on copper samples around 10 years ago [7, 8, 9]. It has been refurbished in 2008 and since then used for samples of the same material. The measurement range was extended to 3

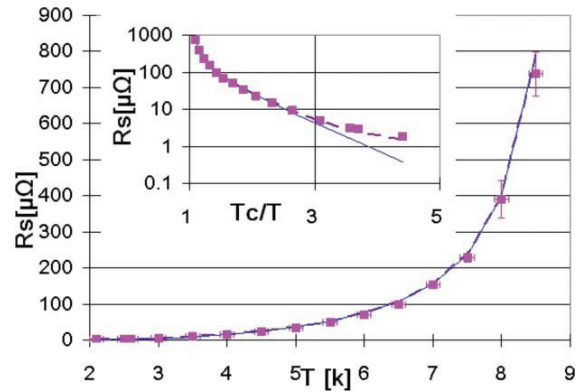


Figure 6: Surface resistance as a function of sample temperature for a bulk niobium sample brazed onto a copper substrate. The line shows the BCS fit [6].

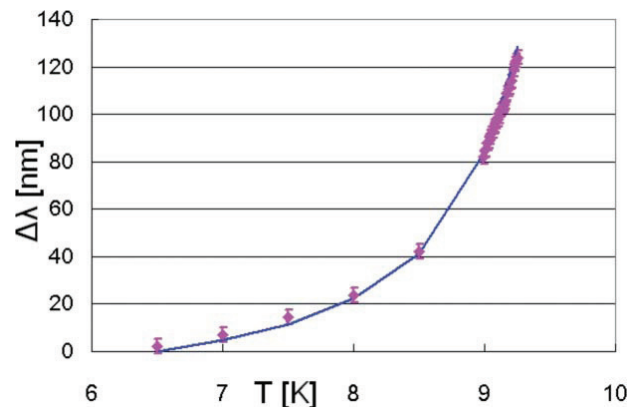


Figure 7: Penetration depth change versus sample temperature for a bulk niobium sample brazed to a copper substrate. The line shows the BCS fit [6].

different frequencies and also the critical field of the samples has been investigated.

In the Quadrupole Resonator the cover plate of a cylinder attached to the cavity in a coaxial structure serves as sample, see Figure 8. Inside this coaxial structure the RF fields are exponentially decaying. This ensures that the power dissipated inside this 1 mm gap and especially at the end flange and joint of the sample cylinder is negligible. This is true for all excitable TE_{21} -like modes up to 2.0 GHz [14]. In principal 5 modes could be excited and used for RF measurements. At CERN equipment for 400, 800 and 1200 MHz is available. Note that RF equipment like amplifiers or circulators is usually narrow band. To perform tests at the three frequencies two different pre-amplifiers (each 5 W, one covering the range up to 500 MHz, the other one the range between 700 and 2200 MHz) and three different main amplifiers (500 W for 400 MHz and 200 W for 800 MHz and 1200 MHz) are used. For each frequency a dedicated circulator is needed. The rest of the used RF equipment covers the whole frequency range.

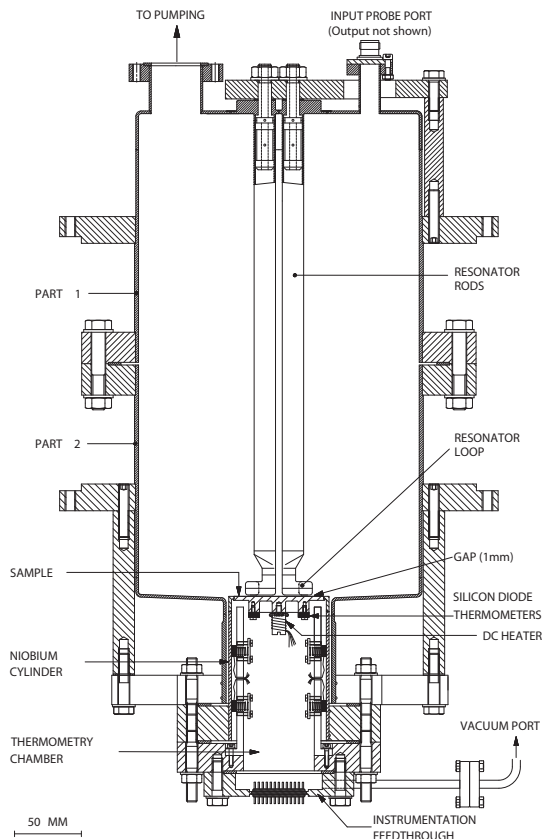


Figure 8: Layout of the niobium Quadrupole Resonator with mounted sample cylinder and a thermometry chamber housing a DC heater (resistor) and temperature sensors [9].

Six calibrated silicon diodes are placed inside the thermometry chamber. Four of them are directly placed below the position of maximum magnetic field on the sample, while two of them are pressed by a piston to the inner wall of the sample cylinder. These two diodes are therefore at a position of lower temperature. This allows to derive the thermal conductivity if sample and sample cylinder are made of the same material [2].

The host cavity consists of two 2 mm thick niobium cans for convenient handling and cleaning of the device. These cans are flanged to each other in the middle of the resonator, where the screening current on the cavity surface vanishes for the modes at 400 and 1200 MHz. For the 800 MHz mode the screening current has a maximum at this position. Since the field is strongly concentrated around the rods in the middle of the resonator, excitation and measurements at 800 MHz are not perturbed by losses at this flange. They are so low that the system remains strongly overcoupled at fields up to 40 mT at 800 MHz. The maximum field at the flange between the upper and the lower can is only 0.53% of the maximum field on the sample.

Surface Impedance

So far the Quadrupole Resonator has been used with bulk niobium and niobium on copper samples. A reactor grade ($RRR \approx 50$) bulk niobium sample was chemically etched (BCP). Precautions were taken that the acid temperature did not exceed 15°C to avoid higher surface resistance caused by hydrides [15]. A niobium film was sputtered with a normal incident angle to a copper substrate and first tested in 1998. The sample was since then kept under normal air, before having been tested again in 2011. Both samples were rinsed with ultrapure water at ≈ 5 bar before being mounted to the Quadrupole Resonator.

Material parameters are derived from least square BCS fits to penetration depth measurements, similar to the ones obtained for the sapphire loaded cavity displayed in Figure 7. The values derived for the Quadrupole Resonator samples are shown in Table 2. They could be better predicted for the the niobium on copper sample. Here the uncertainty in $\Delta\lambda_0$ is derived from the standard deviation from three measurements at 400, 800, 1200 MHz. The bulk niobium sample has a lower thermal conductivity than the niobium on copper sample. The uncertainty in the temperature distribution on the sample and its effect on the obtained value $\Delta\lambda_0$ give the higher uncertainty. The residual resistance ratio RRR was calculated from the empiric relation

$$\ell[nm] = 2.7 \cdot RRR \quad (11)$$

while the Ginzburg Landau parameter κ is derived from [16],

$$\kappa = \frac{\lambda(T, l)}{\xi_{GL}} = \frac{2\sqrt{3}}{\pi} \frac{\lambda(T, l)^2 \cdot (1 - (T/T_c)^2)}{\xi_0 \lambda_L}. \quad (12)$$

This expression is obtained from the fact that the BCS and the Ginzburg Landau coherence lengths ξ_0 and ξ_{GL} are both correlated to the fluxoid quantum Φ_0 [17].

The derived parameters have been used to analyze data of the surface resistance R_S of both samples. Figures 9 and 10 display R_S for low field (<15 mT) in the temperature range between 2 and 10.6 K.

Above $T_c = 9.25$ K all curves are flat, because in the normal conducting regime the surface resistance only slightly depends on temperature. In this temperature regime the

Table 2: Material parameters used for the data analyses of the surface resistance and the critical field. Values are obtained from least square BCS fits to penetration depth measurements

Sample	λ_0 [nm]	RRR	κ (0 K)
Bulk niobium	36-44	26-86	1.13-1.69
Niobium on copper	64.7 ± 0.7	7.6 ± 0.3	3.65 ± 0.08

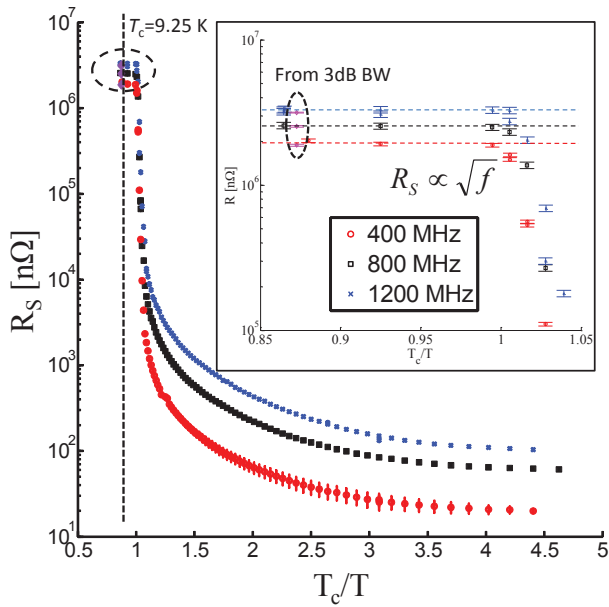


Figure 9: Surface resistance of a bulk niobium sample for three frequencies at low field (<15 mT) as a function of temperature. In the normal conducting regime above T_c the surface resistance was also derived from 3 dB bandwidth measurements.

surface resistance of the sample R_S can also be derived from a non-calorimetric 3 dB bandwidth measurement. If the sample is normal conducting the coupling changes from over to undercoupled and a precise measurement of R_S by the 3 dB bandwidth method is possible [10].

The residual resistance depends on frequency for both samples. For the bulk niobium sample the residual resistance scales identically to the BCS resistance approximately quadratically if an additional non frequency dependent residual surface resistance of $\approx 7 \text{ n}\Omega$ is assumed. For the niobium on copper sample the scaling is smaller than quadratic, indicating other loss mechanisms.

The field dependency of the surface resistance, displayed in Figure 11 for niobium and in Figure 12 for niobium on copper also gives a hint for different loss mechanisms. While the niobium curves show a quadratic increase with field, the Nb on Cu curves show an exponential increase going into saturation for higher fields.

Data of the niobium sample consisting of 181 quadruples (R_S , B , f , T) has been analyzed by a least squares fit to a recently published model [18, 19, 20] in the following referred to as "percolation model". An error $\Delta R/R$ of 4% was assumed for all data points.

All parameters derived from penetration depth measurements, Table 2 were set constant. The percolation model allows for an increasing surface resistance with field already for temperatures below the percolation temperature T' . This effect is not found in the data. Therefore it is assumed to be negligible and this contribution is set to zero. The residual, the BCS and the field dependent (non lin-

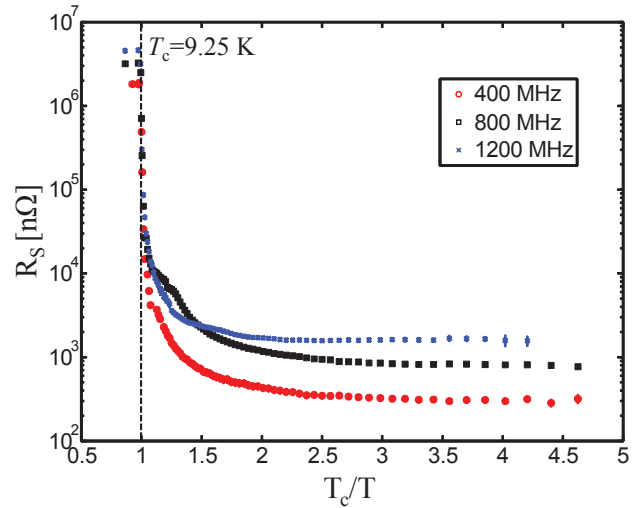


Figure 10: Surface resistance of a niobium film on copper sample for three frequencies at low field (<15 mT) as a function of temperature.

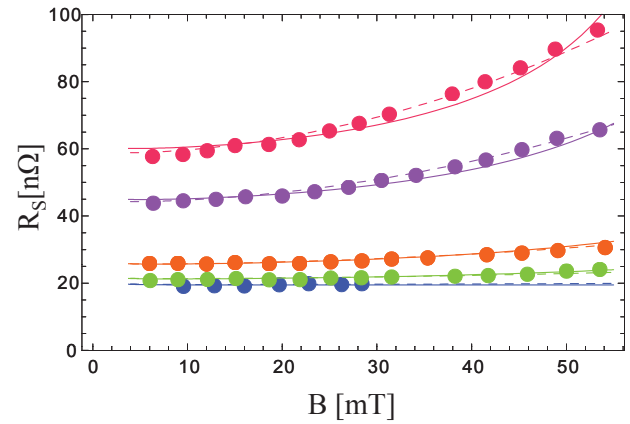


Figure 11: Surface resistance of a bulk niobium sample at 400 MHz for 2 K (blue), 2.5 K (green), 3 K (orange), 4 K (magenta) and 4.5 K (red). Solid curve: Fitting result from percolation model [18]. Dashed curve: Fitting result assuming a quadratic factorization of the BCS resistance.

ear) resistance should all follow the same frequency dependency and are therefore fitted to the same parameter k . Further fit parameters are the penetration depths of the residual Δy and the non-linear resistance Δx , a purely ohmic and therefore field, frequency and temperature independent contribution $R_{\text{Res}2}$ and the superconducting energy gap Δ .

In addition, the data has been analyzed using a simple quadratic factorization of the BCS resistance instead of the non-linear resistance from the percolation model

$$R = R_{\text{BCS}} \left(1 + \gamma \left(\frac{B_p}{B_c} \right)^2 \right). \quad (13)$$

where $B_c=190 \text{ mT}$ is the thermodynamic critical field.

The derived fit parameters for both models can be found in Table 3. In the Quadrupole Resonator the local R_S on the

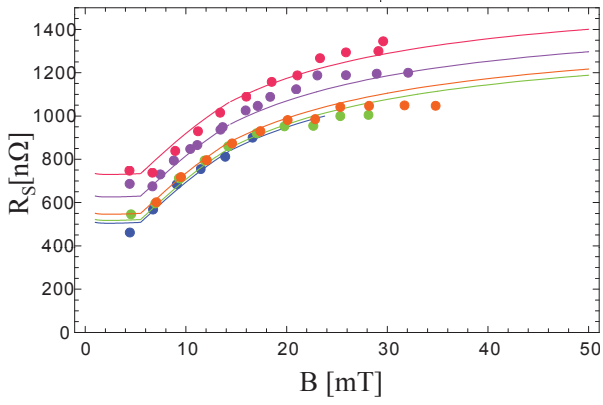


Figure 12: Surface resistance of a niobium on copper sample at 800 MHz for 2.1 K (blue), 2.5 K (green), 2.9 K (orange), 3.5 K (magenta) and 4 K (red).

sample is under-estimated from the average R_S by a factor of 0.55. This has been included in the analyses, assuming a quadratic increase of R_S with B which is well found in the data. A detailed description how to correlate the measured value R_S to its local value can be found in [18].

The analyzed data of the niobium on copper sample consisting of 157 quadruples (R_S , B , f , T) cannot be reasonably fitted by one of the models used for the bulk niobium data. Two effects need to be included: The exponential increase can be explained by including losses from interface tunnel exchange between the superconductor and the adjacent oxides [21], while non quadratic losses can be explained by hysteresis [22]. A detailed analysis of the data will be presented elsewhere [23].

Critical Field

Calorimetric systems not only enable to measure the surface impedance of the samples attached. Also the critical field under RF of the samples can be investigated. One can

Table 3: Parameters derived for least square fits to two different models for the surface resistance

Parameter	Percolation Model Fit	Quadratic BCS fit	Literature value
T' [K]	2.06	-	2.015 [18]
k	1.96	1.95	2 [13]
Δy [nm]	7.2	7.9	-
Δx [nm]	106.0	-	-
R_{Res2} [nΩ]	7.25	7.21	-
Δ [K]	18.9	18.7	16-18 [13]
γ	-	20.4	-
Quadruples			
(R_S , B , f , T)	181	181	
χ^2	213.6	192.6	-

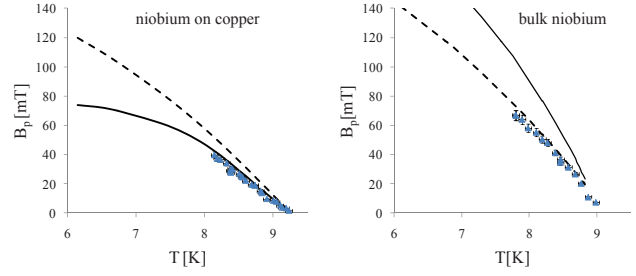


Figure 13: Critical field under RF (short pulses). Left: Niobium on copper sample. Right: Bulk niobium sample. Solid line: Prediction from vortex line nucleation model. Dashed line: Prediction from Ginzburg Landau model.

easily determine, without further diagnostics, if a quench happened on the host cavity or on the sample, simply by measuring the sample temperature the moment the quench occurs. If the temperature rises above T_c the quench was on the sample, otherwise it must have been on the host cavity.

The critical field under RF exposure has been investigated using pulses just long enough that the stored energy in the cavity reaches steady state (pulse length ≈ 2 ms) and in continuous wave (CW) operation. Different field levels and dependencies on frequency have been found.

If short pulses are used the critical field is found to be independent on frequency. Critical fields above the thermodynamic critical B_c have been measured [24, 25, 26]. The results are explained by a superheating field H_{sh} either derived from Ginzburg-Landau-Theory [27, 28] or by a thermodynamic energy balance [29, 30, 31].

For the data analysis the vortex line nucleation model (VLNM) [31] and the approximate formulas from [28] in the following named "Ginzburg Landau model" (GLM) are used. For both models H_{sh} depends on the Ginzburg Landau parameter κ . Its value is calculated from equation 12, with $\lambda(T, l)$ derived from measurement and $\xi_0 = 39$ nm and $\lambda_L = 32$ nm taken from literature [13].

For high values of κ the GLM predicts H_{sh} higher than the VLNM. This is the case for the niobium on copper sample. For the bulk Nb sample H_{sh} is predicted to be higher for the VLNM. For both samples the lower limitation is met. Therefore it is possible that both mechanisms set limits to the maximum field under RF in superconducting cavities, see Figure 13.

To measure the critical field in CW, first B_p is set to a fixed level. Then the sample temperature is slowly raised until the quench occurs. Usually a sudden temperature raise above T_c is observed the moment the quench occurs.

The quench field is found to scale with frequency like $B_p \propto f^{-0.46 \pm 0.13}$, see Figure 14. This cannot be explained by a commonly used model based on a normal conducting defect surrounded by the superconductor. This model predicts $B_p \propto f^{-0.25}$ [1]. The fact that B_p vs. $1-(T_c/T)^2$ gives a straight line is an indication that a field limitation is found. The fields are limited to lower values compared to

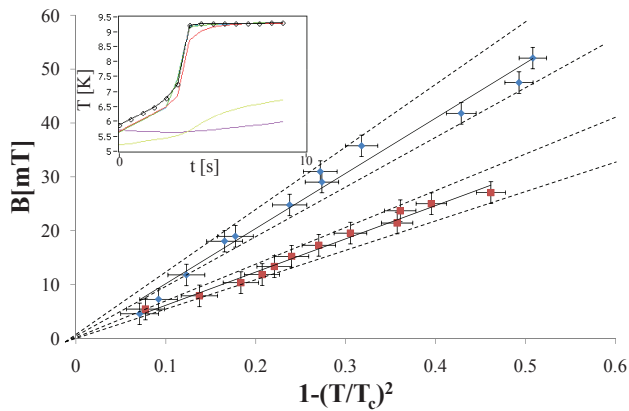


Figure 14: Quench field in CW measured at 1200 (red squares) and 400 MHz (blue squares). Top left: Usually a sudden temperature raise above T_c is observed the moment the quench occurs.

pulsed operation. This can be explained by a local defect heating its surrounding area. When the temperature in the vicinity of the defect exceeds the field dependent critical temperature the quench occurs.

SUMMARY AND OUTLOOK

Currently there are three calorimetric systems for the RF characterization of superconducting samples in use. Two of them, the TE₀₁₁/TE₀₁₂ cavity from IPN Orsay/CEA Saclay and the sapphire loaded cavity from JLAB have been recently commissioned, while the third one, the Quadrupole Resonator, has been recently refurbished.

All systems are equipped with high resolution temperature sensors (≈ 0.1 mK), enabling them to detect a heating corresponding to $R_S \approx 1$ n Ω at $B_p = 5$ mT, see Table 4. The highest field on sample B_p has been achieved by the Quadrupole Resonator, limited by a quench at 60 mT. The sapphire loaded cavity is currently limited by the available amplifier power, while TE₀₁₁/TE₀₁₂ cavity has achieved fields up to 40 mT in the past.

So far none of the three systems has been used for measurements of materials other than niobium. The results on the niobium samples prove the capability of the calorimetric method and the three devices. The cavities are now commissioned and ready for measurements of new materials like Nb₃Sn, Mg₂B [32] or multilayers [33] of superconducting and insulating layers.

To reveal the intrinsic properties of the samples under test, it is necessary to correlate the RF measurements to surface analyses measurements. This will be done for the samples tested by the Quadrupole Resonator in the future.

The high precision of the calorimetric method has recently gained much attention and further instruments are currently under development in several laboratories.

Table 4: Overview of calorimetric systems for the RF characterization of superconducting sample currently in use.

	TE ₀₁₁ / TE ₀₁₂ cavity	Sapphire loaded cavity	Quadrupole Resonator
f [GHz]	4.0/5.6	7.5	0.4/0.8/1.2
Sample diameter [cm]	12	5	7.5
Max. field obtained on sample B_p [mT]	40	14	60
Resolution at $B_p=5$ mT [n Ω]	1.43	1.2	0.44

ACKNOWLEDGMENT

The authors like to thank all the members of the BE/RF/KS section and everybody else who contributed to the refurbishment of the Quadrupole Resonator. The work of S. Calatroni and S. Forel (preparation of samples) and the operators from TE/CRG is highly appreciated. Thanks to Ernst Häbel for designing and explaining the Quadrupole Resonator. Special thanks to B. Xiao, G. Martinet and M. Fouaidy for providing information about their work and results.

One of us (TJ) is also indebted to the German Ministry of Education and Research for being awarded a grant by the German Doctoral Program at CERN (Gentner - Program).

REFERENCES

- [1] H. Padamsee, T. Hays, and J. Knobloch, *RF superconductivity for accelerators; 2nd ed.* Weinheim: Wiley, 2008.
- [2] T. Junginger, W. Weingarten, and C. Welsch, "RF characterization of superconducting samples." in *Proceedings of the 14th International Workshop on RF Superconductivity, Berlin, Germany, 2009.*
- [3] M. Fouaidy *et al.*, "New Results on RF Properties of Superconducting Niobium Films Using a Thermometric System," in *Proceedings of the 8th European Particle Accelerator Conference, Paris, France, 2002.*
- [4] S. Chel *et al.*, "Surface Resistance Measurements of Superconducting Samples with Vacuum Insulated Thermometers," in *Proceedings of the 5th European Particle Accelerator Conference, Stockholm, Sweden, 1998.*
- [5] G. Martinet *et al.*, "Development of a TE₀₁₁ cavity for thin-films study," *Proceedings of the 14th International Workshop on RF Superconductivity, Berlin, Germany, 2009.*
- [6] B. P. Xiao *et al.*, "Radio frequency surface impedance characterization system for superconducting samples at 7.5 GHz," *Review of Scientific Instruments*, vol. 82, no. 5, p. 056104, 2011.
- [7] E. Brigant, E. Häbel, and E. Mahner, "The Quadrupole Resonator, Design Considerations and Layout of a New Instrument for the RF Characterization of Superconducting Sur-

- face Samples,” in *Proceedings of the 6th European Particle Accelerator Conference, Stockholm, Sweden, 1998*.
- [8] E. Chiaveri *et al.*, “The Quadrupole Resonator: Construction, RF System Field Calculations and First Applications,” in *Proceedings of the 6th European Particle Accelerator Conference, Stockholm, Sweden, 1998*.
- [9] E. Mahner *et al.*, “A New Instrument to Measure the Surface Resistance of Superconducting Samples at 400 MHz,” *Rev. Sci. Instrum.*, vol. 74, 2003.
- [10] T. Junginger and N. Schwerg, “Q-Factor of the Quadrupole Resonator with Niobium Sample,” <https://edms.cern.ch/document/1153270/1>, Tech. Rep., 2011.
- [11] G. Ciovati, “Private communication; J. Halbritter, Externer Bericht 3/69-2 (Kernforschungszentrum, Karlsruhe, 1969); Externer Bericht 3/70-6 (Kernforschungszentrum, Karlsruhe, 1970); J. Halbritter, *Z. Phys.* 266 (1974) 209.”
- [12] —, Ph.D. dissertation, Old Dominion University, 2005.
- [13] J. P. Turneaure, J. Halbritter, and H. A. Schwetman, “The Surface Impedance of Superconductors and Normal Conductors: The Mattis-Bardeen Theory,” *Journal of Superconductivity*, vol. 4, 1991.
- [14] H. H. Meinke *et al.*, *Taschenbuch der Hochfrequenztechnik; 4. Aufl.* Berlin: Springer, 1986.
- [15] H. Padamsee, *RF superconductivity: Science, Technology, and Applications*. New York, NY: Wiley, 2009.
- [16] T. Junginger, “Intrinsic Limitations of Niobium under RF,” in *Proceedings of the Fourth International Workshop on: Thin Films and new Ideas to push the Limits of RF Superconductivity Legarno National Laboratories (Padua)*, 2010.
- [17] M. Tinkham, *Introduction to Superconductivity*. Dover Publications, 2004.
- [18] W. Weingarten, “A two-fluid model description of the Q-slope and Q-drop as observed in niobium superconducting accelerating cavities, oai:cdsweb.cern.ch/record/1336494,” Mar 2011.
- [19] —, “On the Field Dependent Surface Resistance observed in Superconducting Niobium Cavities,” in *Proceedings of the 14th International Workshop on RF Superconductivity, Berlin, Germany, 2009*.
- [20] —, “Field-dependent surface resistance for superconducting niobium accelerating cavities,” *Submitted to Phys. Rev. ST. AB 12.4.2011*.
- [21] J. Halbritter, “Transport in superconducting niobium films for radio frequency applications,” *Journal of Applied Physics*, vol. 97, 2005.
- [22] C. Durand *et al.*, “Non Quadratic RF Losses in Niobium Sputter Coated Accelerating Structures,” *IEEE Transactions on Applied Superconductivity*, vol. 5, no. 2, 1995.
- [23] T. Junginger *et al.*, “RF and surface properties of superconducting samples,” in *Proceedings of the 2nd International Particle Accelerator Conference, San Sebastian, Spain (to be published)*, 2011.
- [24] T. Hays and H. Padamsee, “Measuring the RF Critical Field of Pb, Nb, and Nb₃Sn,” in *Proceedings of the 1997 Workshop on RF Superconductivity, Abano Terme (Padova), Italy, 1997*.
- [25] N. R. A. Valles and M. U. Liepe, “Exploring the maximum superheating magnetic fields of niobium,” in *Proceedings of the 14th International Conference on RF Superconductivity, Berlin, Germany, 2009*.
- [26] —, “Temperature dependence of the superheating field in niobium,” *arXiv:1002.3182v1 [cond-mat.supr-con]* 16 Feb 2010.
- [27] J. Matricon and D. Saint-James, “Superheating fields in superconductors,” *Physics Letters A*, vol. 24, 1967.
- [28] M. K. Transtrum, G. Catelani, and J. P. Sethna, “Superheating field of superconductors within Ginzburg-Landau theory,” *Phys. Rev. B*, vol. 83, no. 9, 2011.
- [29] T. Yogi, G. J. Dick, and J. E. Mercereau, “Critical rf Magnetic Fields for Some Type-I and Type-II Superconductors,” *Phys. Rev. Lett.*, vol. 39, no. 13, 1977.
- [30] K. Saito, “Critical Field Limitation of the Niobium Superconducting RF Cavity,” *Proceedings of the 10th International Conference on RF Superconductivity, Tsukuba, Japan, 2001*.
- [31] —, “Theoretical Critical field in RF Application,” *Proceedings of the 11th International Conference on RF Superconductivity, Hamburg, Germany, 2003*.
- [32] V. Palmieri, “New materials for superconducting radiofrequency cavities,” in *Proceedings of the 10th Workshop on RF Superconductivity, Tsukuba, Japan, 2001*.
- [33] A. Gurevich, “Enhancement of rf breakdown field of superconductors by multilayer coating,” *Applied Physics Letters*, vol. 88, 2006.